ACS APPLIED MATERIALS & INTERFACES

Research Article

www.acsami.org

Efficient Luminescence of Long Persistent Phosphor Combined with Photonic Crystal

Xiaodi Shi,[†,‡] Lei Shi,[§] Mingzhu Li,[*,†] Jue Hou,[†,‡] Linfeng Chen,[†,‡] Changqing Ye,[†,‡] Weizhi Shen,[†,‡] Lei Jiang,[†] and Yanlin Song[*,†]

[†]Key Laboratory of Organic Solid, Key Laboratory of Green Printing, Institute of Chemistry, Chinese Academy of Sciences, Beijing 100190, P. R. China

[‡]Graduate University of Chinese Academy of Sciences, Beijing 100049, P. R. China

[§]Department of Physics and Key Laboratory of Micro and Nano Photonic Structures, Fudan University, Shanghai 200433, P. R. China

Supporting Information

ABSTRACT: In this paper, the luminescence properties of the long persistent phosphor (LPP) were apparently improved by combining with photonic crystal (PC). An optimized PC can double the afterglow intensity and prolong 1.7 times of the afterglow time of $SrAl_2O_4$: Eu, a commercially available LPP, without any dopants. These results were ascribed to the stopband effect of the PC. The PC combined LPP structure was beneficial for the applications of LPP in emergency indication which called for brighter afterglow intensity and longer afterglow time.

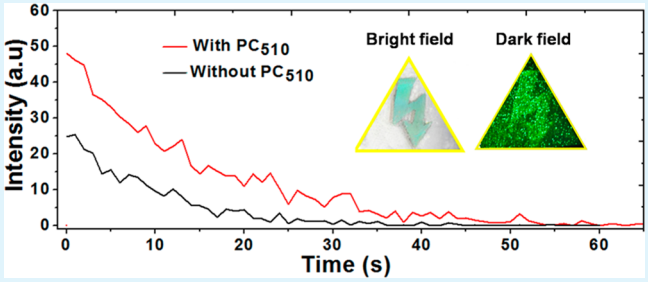

KEYWORDS: *photonic crystal, long persistent phosphor, afterglow intensity, afterglow time*

1. INTRODUCTION

The long persistent phosphor (LPP) is a kind of photoluminescence material which exhibits particular light storing and releasing properties.[1−3] Nowadays, the LPP can remain visible for hours without any power source, which ensures the safety during everyday operations and in an event of emergency.[4] The enhancement of the afterglow intensity and the prolongation of the afterglow time of the LPP stimulate its applications spreading over wide fields including safety indicator,[5] display,[6] solar cell,[7−9] in vivo image,[10] detector of the high energy radiation,[11] and so on. However, the current methods to improve the luminescence properties of the LPP are always complicated and expensive, which are mostly realized by doping with rare earth ions or varying the synthesis process and always need high reaction or calculating temperatures.[12−15] It is still a challenge to find a facile and low-cost way to improve the LPP luminescence properties. As known, spontaneous emission is a fundamental process resulting from the interactions between radiation and matter. The performance of spontaneous emission depends on both the excited atom and the utilization environment. The luminescence of the LPP shares the same mechanism. Photonic crystal (PC) is a promising material which can change the utilization environment and enhance the emission of the fluorescence emitter.[16,17] PC has periodic variations in the dielectric permittivity at the wavelength scale. Density of state in PC is redistributed, so that PC can serve as a dielectric mirror to enhance the intensity of emission light.[18−20] Consequently, PC is a promising material for the amplification of spontaneous emission as well as the control of the propagation of light.[21−29] In our previous work, PC was used to enhance the emission intensity of chemiluminescence (CL) or fluorescence and improve the fluorescence-based detection sensitivity.[30−32] Herein, we introduced PC into the LPP system and achieved 2-fold enhancement of the afterglow intensity and 1.7-fold prolongation of the afterglow time. The results were beneficial for the applications of LPP in emergency indication which called for brighter afterglow intensity and longer afterglow time.

2. EXPERIMENTAL SECTION

2.1. Materials. The long persistent phosphor (LPP) SP-6 ($SrAl_2O_4$: Eu) was purchased from Dalian Lu-ming light Co., Ltd.; polydimethylsiloxane (PDMS) was purchased from Dow Corning; all the other reagents were purchased from Beijing Chemical Works. They were all used directly without further purity except for the distilled styrene (St), methyl methacrylate (MMA), and acrylic acid (AA).

2.2. Preparation of PC and the LPP Film. The PCs were prepared according to the literature.[33,34] First, the monodispersed polymer latex spheres poly(styrene-methyl-methacrylate-acrylic acid) (poly(St-MMA-AA)) were synthesized by the emulsion polymerization method.[33] The PC was prepared by vertical deposition of the monodispersed polymer latex spheres on glass slides at constant humidity (80%) and temperature (80 °C).[34] The glass slides were pretreated with H_2O_2-sulfuric cleaning solution, rinsed with ultrapure water, and dried in a stream of nitrogen to ensure its hydrophilicity.

Received: November 27, 2013
Accepted: April 9, 2014
Published: April 9, 2014

Herein, $SrAl_2O_4$: Eu, a commercially available LPP, was chosen to investigate the influence of PC on the LPP luminescence properties for its steady light emission properties. The $SrAl_2O_4$: Eu was first mixed with PDMS (monomer and initiator). The mixtures were spin coated on pretreated glass slide and then solidified under 80 °C for 2 h to form the uniform PDMS polymer film containing LPP (LPP film). Parameters associated with LPP film thickness and the excitation light intensities were both optimized (Figure S1).

2.3. Characterization. The SEM images were obtained by a field emission SEM (JEOL JSM-6700, Japan). Reflection spectra were recorded on a U-4100 UV−visible spectrophotometer (Hitachi, Japan). Luminescence spectra were measured by F-4500 fluorescence spectrophotometer (Hitachi, Japan) with the lamp turned off. The XRD pattern was characterized by X-ray diffraction (XRD) using a Rigaku X-ray diffractometer with graphite monochromatized Cu Ka irradiation (λ = 1.54056 Å). The photographs were captured by digital camera (Nikon, D90). The film thickness of PDMS was recorded by the step profiler (Kosaka, ET4000AK). The power of the sunlight modulator power was characterized by light intensity meter (FZ-A).

3. RESULTS AND DISCUSSION

The LPP combined PC structure was constructed as illustrated in Figure 1a. The PC was fabricated from the monodispersed

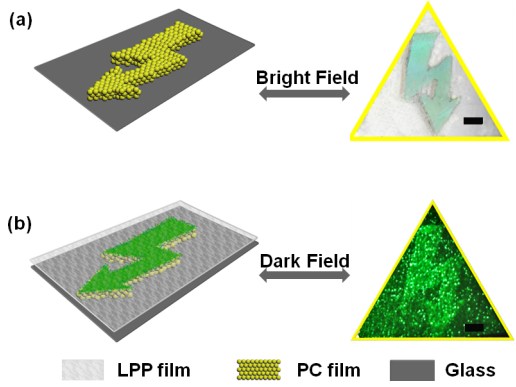

Figure 1. (a) The schematic illustration of the PC layer formed by self-assembly of the polymer latex spheres onto a glass slide. The PC film was shaped following the warning sign. The digital photo of the PC (image on the right) showed athe green color in bright field. (b) The schematic illustration of PC enhanced LPP luminescent intensity. The PC served as the background substrate to improve the luminescence properties of the LPP. The warning sign was arisen from the brighter luminescence of areas with PC (image on the right). The scale bar was 3 mm.

poly(St−MMA−AA) latex spheres via the vertical deposition method at constant humidity (80%) and temperature (80 °C).[34] The PC layer was shaped following the warning sign. The image on the right of Figure 1a was the optical image of the optimized PC film, which showed brilliant green color under sunlight due to its Bragg scattering. Herein, $SrAl_2O_4$: Eu, a commercially available LPP, was used to demonstrate that the introduction of PC could improve the luminescence properties of the LPP. PDMS was chosen as the carrier of the LPP for its good light transparency property. Besides, PDMS have no light interference in the wavelength range of $SrAl_2O_4$: Eu excitation and emission light, so the luminescence properties of $SrAl_2O_4$: Eu would not be affected by PDMS. The $SrAl_2O_4$: Eu was mixed with PDMS and solidified to form a uniform PDMS polymer film containing LPP (LPP film). Using the PC film as a background substrate, the enhancement effect of PC to $SrAl_2O_4$: Eu luminescence properties was characterized. The schematic illustration of Figure 1b presented the enhancement of the $SrAl_2O_4$: Eu luminescence intensity by the PC. The green pattern stood for the areas of the LPP film with PC layer, which showed brighter luminescence intensity in dark field (Figure 1b). Moreover, the energy storing - energy releasing cycles of the LPP combined PC system kept steady luminescence properties and could be used repeatedly (Fifteen cyclic processes were shown in Figure S2.).

Herein, PDMS was chosen as the carrier of $SrAl_2O_4$: Eu to form the uniform LPP film. Figure 2a showed the XRD pattern

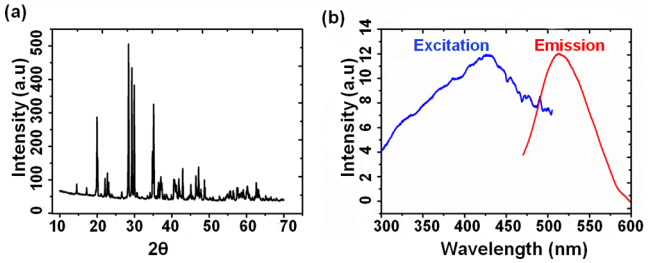

Figure 2. (a) The XRD pattern of the host matrix of $SrAl_2O_4$: Eu, which was well matched with the monoclinic $SrAl_2O_4$ phase pattern. (b) The excitation and emission spectra of $SrAl_2O_4$: Eu. It was seen that $SrAl_2O_4$: Eu had broadband excitation and emission spectra.

of the host matrix of $SrAl_2O_4$: Eu. According to the joint committee on powder diffraction standards (JCPDS), the XRD pattern of the phosphor was well matched with the monoclinic $SrAl_2O_4$ phase pattern.[3] The $SrAl_2O_4$: Eu had a broadband absorption from 300 to 500 nm (Figure 2d, blue line) and gave off greenish emission with broadband spectrum centered at ca. 510 nm (Figure 2b, red line). This was corresponding to transition between the 5d and 4f orbital gaps of Eu^{2+} in the host matrix $SrAl_2O_4$.[35] Therefore, the sunlight simulator which had a broadband emission light was used as excitation light source. Parameters associated with the excitation light intensity were optimized (Figure S1a).

To investigate the influence of PCs on the luminescent properties of $SrAl_2O_4$: Eu, PCs were assembled from the monodispersed latex spheres poly(St−MMA−AA). The surface morphologies of the PCs were characterized by JEOL JSM-6700 field emission scanning electron microscope (SEM). The diameters of the latex spheres were respectively 180 nm, 195 nm, 205 and 245 nm. Figure 3 showed the SEM images of the as-prepared PCs, which presented the ordered face-centered cubic (FCC) structure. The close-packed arrangement could extend over a large area, which provided the possibility for its applications in optical devices. The two-dimensional fast Fourier transform (FFT) images presented symmetrical lattice array (Figure 3, insets), which confirmed that the latex spheres were arranged in a high-degree of order.[36] The periodic structure of PCs gave rise to a dielectric stopband, which dramatically modified the light propagation and spontaneous emission.

The reflection spectra of the as prepared PCs were centered at 484 nm (PC_{484}), 510 nm (PC_{510}), 530 nm (PC_{530}), and 657 nm (PC_{657}) respectively, which revealed the position of their stopbands (Figure 4). They were respectively assembled by polymer latex spheres of 180 nm, 195 nm, 205 and 245 nm in diameter. Insets were the corresponding digital photos of the PCs. They all showed uniform and brilliant structure color in a large scale in sunlight, which confirmed the good quality of the

dx.doi.org/10.1021/am501420w | ACS Appl. Mater. Interfaces 2014, 6, 6317−6321

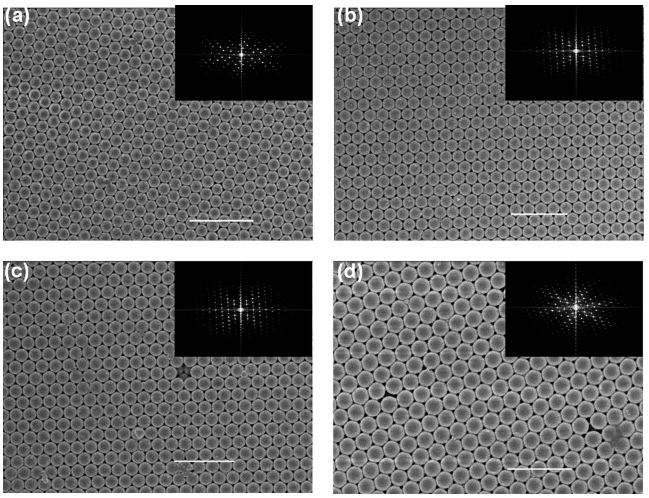

Figure 3. The SEM images of the PCs. The inset depicting the corresponding fast Fourier transform (FFT) spectra of the SEM images. The symmetrical lattice array indicated the highly ordered structures of the PCs. The diameters of the latex spheres were 180 nm (a), 195 nm (b), 205 nm (c), and 245 nm (d) respectively. Their scale bars were 1 μm.

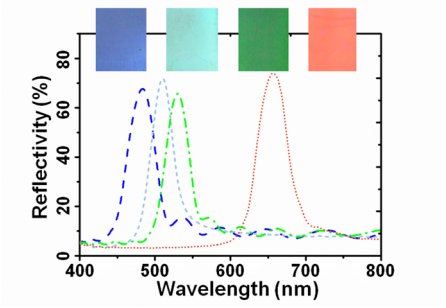

Figure 4. The reflection spectra of the PCs, marked respectively as PC_{484}, PC_{510}, PC_{530}, and PC_{657} according to their stopbands. Insets were the digital photos of the corresponding PCs, which presented brilliant structure color under sunlight.

PCs. The emission light wavelength of $SrAl_2O_4$: Eu was centered at 510 nm, which was matched with the stopband of PC_{510}.

The enhancement effect of PC to the afterglow intensity of $SrAl_2O_4$: Eu was then characterized, which was defined as the ratio of the initial afterglow intensity at the maximum emission wavelength of $SrAl_2O_4$: Eu with and without PC. Initial afterglow intensity was collected 10 s after the excitation light source was removed to ensure the data consistency. The enhancement effects of PCs to the afterglow intensity differed from 1.3 times to 2.0 times (Figure 5a). PC_{510}, the stopband of which was matched with the maximum emission wavelength of $SrAl_2O_4$: Eu, had the highest improvement, which was 2.0 times. The stopband of the PC_{510} was matched with the LPP emission wavelength, light emission within the PC_{510} was forbidden to enter into the PC and was effectively reflected back, and the improvement was the highest. The bandstructure of the PC_{510} was simulated by finite-difference time-domain (FDTD) simulation methods.[37] As is shown in Figure 5b, a clear dip of photon density of state within the LPP emission wavelength range was observed. Apparently, the stopband along the L direction (111) matched the dip of local density of state quite well. The calculated stopband of the PC_{510} was matched

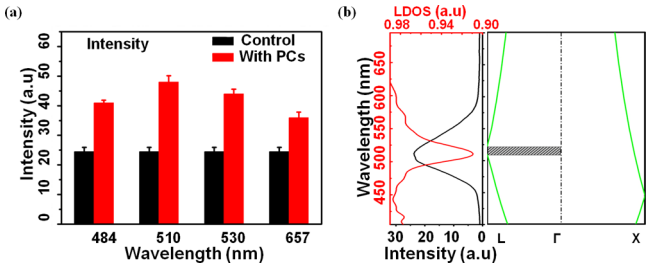

Figure 5. (a) The afterglow intensities of $SrAl_2O_4$: Eu enhanced by PCs with different stopbands. (b) The calculated distribution of local density of state inside the PC_{510} in the range of the $SrAl_2O_4$: Eu emission wavelength range and the calculated stopband of the PC_{510}. The $SrAl_2O_4$: Eu emission wavelength matched well with the calculated stopband.

with the $SrAl_2O_4$: Eu emission wavelength. In the stopband, the propagation of light within the range of the stopband wavelength was inhibited. Thus, the emission light of the $SrAl_2O_4$: Eu could not go through the PC_{510}. The refractive index of latex spheres was set to be 1.59. The diameter of latex spheres was set to be 205 nm, which was slightly larger than 195 nm in the experiment. This may be caused by the non-point touch between the latex spheres.[36]

Another interesting phenomenon was observed that the afterglow time of $SrAl_2O_4$: Eu was also prolonged by PC. The afterglow time was defined as the duration of the afterglow intensity decayed to 10% of its initial afterglow intensity. The prolongation of PC to the afterglow time was defined as the ratio of $SrAl_2O_4$: Eu afterglow time with and without PC. All PCs can prolong the afterglow time with different prolongation factor, from 1.3 times to 1.7 times (Figure 6a). In this work,

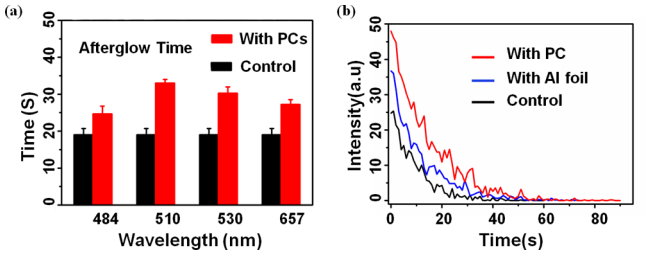

Figure 6. (a) The prolongation of the afterglow time of $SrAl_2O_4$: Eu by PCs with different stopbands. (b) The decay curves of $SrAl_2O_4$: Eu afterglow intensities with the optimized PC (red line), Al foil (blue line), and the control sample (black line).

considering the detecting limitation of the fluorescence spectrometer, only a little amount (0.05%) of LPP was mixed with PDMS to form the LPP film. For application, brighter afterglow intensity can be achieved by improving the content of LPP, e.g., when the content of LPP was improved to 20%, the afterglow intensity was still visible after 3 h's decay (Figure S3). The enhancement effect of reflection mirror (aluminum foil) had been characterized and compared with that of the PC. Its enhancement to afterglow intensity was 1.5 times and prolongation to the afterglow time was 1.3 times, which was lower than those of PC (Figure 6b, blue line and red line). Besides, for PCs, only light in certain wavelength range can be reflected back. This was beneficial for improving the color purity of light, which was more favorable for its application in emergency indication. While for aluminum foil, light in the

dx.doi.org/10.1021/am501420w | ACS Appl. Mater. Interfaces 2014, 6, 6317−6321

whole wavelength range was all reflected back, and the background interference was enhanced.

To understand the luminescence enhancement effect, the E-field plot was calculated in the case of a Gaussian beam (510 nm wavelength) normally incident to the PC. The simulation was performed under the commercial FDTD software (FDTD Solutions).[37] The boundary condition for all the boundary was perfect matching layer. In the reflection simulation, the light source was a Gaussian beam. While in the emission simulation, the light source was an electric dipole. The E field polarization of all the simulations was along the *x*-axis. It was clear that inside the PC, the field intensity decreased rapidly, which corresponded to the band gap effect. The strong light reflected back interfered with the incident one (the emission light of the $SrAl_2O_4$: Eu), which resulted in a standing wave in front of the PC shown in Figure 7a. Because of that, the electric field in a certain place was enhanced. When an electric dipole, $SrAl_2O_4$: Eu, showed green emission peaking at 510 nm (parity-allowed transition of $4f^65d^1$ to $4f^7$ (8S) of Eu^{2+} caused by the thermal disturbance or external field stimulation[2,3]), whose emission frequency was the maximum in the standing wave (black arrow in Figure 7b), the radiation pattern (red line in Figure 7b) was strongly modified comparing with the radiation pattern (black line in Figure 7a) for the case of the same emitter located in the vacuum. Therefore, the luminescence property of $SrAl_2O_4$: Eu depended on both the character of the material and the utilization environment. For $SrAl_2O_4$: Eu with PC, the enhancement effect of the afterglow intensity was assigned to the utilization environment modified by the PC.[16,24−26] The total emission intensity was increased because of the high electric field intensity. Most of the emission light emitted to the free space, and the direction was normal to the surface of the PC because of the stopband effect. The reason for the prolonged afterglow time was also associated with the amplified spontaneous emission of $SrAl_2O_4$: Eu by the PC and lead to longer afterglow time.[16] Besides, as shown in Figure 2d, there was certain overlap between the excitation and emission spectra of $SrAl_2O_4$: Eu.[2] For $SrAl_2O_4$: Eu with PC, during the luminescence decay process, the emission light reflected back by PC would be reabsorbed by $SrAl_2O_4$: Eu, which further excited $SrAl_2O_4$: Eu to give off light, and lead to longer afterglow time. For PCs with mismatched stopbands, the enhancement effect mainly resulted from the multiple scattering. As the diameters of the polymer latex spheres were very close, their enhancement effects were similar.

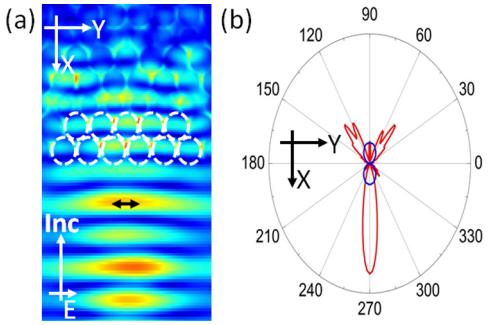

Figure 7. (a) The E-field plot when a Gaussian beam normally incident to the PC. (b) The radiation pattern of an electric dipole (shown as the black arrow) located in front of the PC (red curve) and located in vacuum (blue curve).

4. CONCLUSIONS

In this work, a facile, efficient and recyclable PC combined LPP structure was achieved. It was demonstrated that the optimized PC could almost double the afterglow intensity and prolong 1.7 times of the afterglow time of $SrAl_2O_4$: Eu, a commercially available LPP, without any dopants. This strategy would be of great importance for the application of LPP in security signal, emergency route signage, and various displays which called for brighter afterglow intensity and longer afterglow time.

■ ASSOCIATED CONTENT

Supporting Information

The characterization of the excitation light power, the thickness of the PDMS film, the preparation process of the latex spheres and the assemble of the PCs, the enhancement effect of aluminum foil to the LPP, the decay process of LPP-combined PC structure. This material is available free of charge via the Internet at http://pubs.acs.org.

■ AUTHOR INFORMATION

Corresponding Authors

*Phone/Fax: +86 10-6252 9284. E-mail: ylsong@iccas.ac.cn.
*E-mail: mingzhu@iccas.ac.cn.

Notes

The authors declare no competing financial interest.

■ ACKNOWLEDGMENTS

We gratefully acknowledge financial support from the NSFC (Grant Nos. 51173190, 21003132, 21073203, 91127038, and 21121001), the 973 Program (2013CB933004, 2011CB932303 and 2011CB808400), Beijing Nova Program (Z131103000413051), and the "Strategic Priority Research Program" of the Chinese Academy of Sciences (Grant No. XDA09020000).

■ REFERENCES

(1) Li, Y. Q.; Wang, Y. H.; Gong, Y.; Xu, X. H.; Zhou, M. J. Design, Synthesis and Characterization of an Orange-yellow Long Persistent Phosphor: $Sr_3Al_2O_5Cl_2$: Eu^{2+}, Tm^{3+}. *Opt. Express* **2010**, *18*, 24853.
(2) Kandpal, S. K.; Goundie, B.; Wright, J.; Pollock, R. A.; Mason, M. D.; Meulenberg, R. W. Inverstigation of the Emission Mechanism in Milled $SrAl_2O_4$: Eu, Dy Using Optical and Synchrotrox X-ray Spectroscopy. *ACS Appl. Mater. Interfaces* **2011**, *3*, 3482−3486.
(3) Escribano, P.; Marchal, M.; Sanjuán, M. L.; Gutiérrez, P. A.; Julián, B.; Cordoncillo, E. Low-Temperature Synthesis of $SrAl_2O_4$ by a Modified Sol-Gel Route: XRD and Raman Characterization. *J. Solid State Chem.* **2005**, *178*, 1978−1987.
(4) Wang, Y.; Gong, Y.; Xu, X.; Li, Y. Recent Progress in Multicolor Long Persistent Phosphors. *J. Lumin.* **2013**, *133*, 25−29.
(5) Ueda, J.; Aishima, K.; Nishiura, S.; Tanabe, S. Afterglow Luminescence in $Ce3^+$-Doped $Y_3Sc_2Ga_3O_{12}$ Ceramics. *Appl. Phys. Express* **2011**, *4*, 042602.
(6) Wang, W. X.; Yang, P. P.; Cheng, Z. Y.; Hou, Z. Y.; Li, C. X.; Lin, J. Patterning of Red, Green, and Blue Luminescent Films Based on $CaWO_4$: Eu^{3+}, $CaWO_4$: Tb^{3+}, and $CaWO_4$ Phosphors via Micro-contact Printing Route. *ACS Appl. Mater. Interfaces* **2011**, *3*, 3921−3928.
(7) Hosseini, Z.; Huang, W. K.; Tsai, C. M.; Chen, T. M.; Taghavinia, N.; Diau, E. W. G. Enhanced Light Harvesting with a Reflective Luminescent Down-Shifting Layer of Dye-Sensitized Solar Cells. *ACS Appl. Mater. Interfaces* **2013**, *5*, 5397−5402.
(8) He, W. Z.; Atabaev, T. S.; Kim, H. K.; Hwang, Y. H. Enhanced Sunlight Harvesting of Dye-Sensitized Solar Cells Assisted with Long

Persistent Phosphor Materials. *J. Phys. Chem. C* **2013**, *117*, 17894−17900.
(9) Huang, X. Y.; Han, S. Y.; Huang, W.; Liu, X. G. Enhancing Solar Cell Efficiency: The Search For Luminescent Materials as Spectral Converters. *Chem. Soc. Rev.* **2013**, *42*, 173−201.
(10) Li, Z. J.; Zhang, H. W.; Sun, M.; Shen, J. S.; Fu, H. X. A Facile and Effective Method to Prepare Long-Persistent Phosphorescent Nanospheres and Its Potential Application for In Vivo Imaging. *J. Mater. Chem.* **2012**, *22*, 24713−24720.
(11) Kowatari, M.; Koyama, D.; Satoh, Y.; Iinuma, K.; Uchida, S. The Temperature Dependence of Luminescence From a Long-Lasting Phosphor Exposed to Ionizing Radiation. *Nucl. Instrum. Methods Phys. Res., Sect. A* **2002**, *480*, 431−439.
(12) Allix, M.; Chenu, S.; Véron, E.; Poumeyrol, T.; Boudjelthia, E. A. K.; Alahraché, S.; Porcher, F.; Massiot, D.; Fayon, F. Considerable Improvement of Long-Persistent Luminescence in Germanium and Tin Substituted $ZnGa_2O_4$. *Chem. Mater.* **2013**, *25*, 1600−1606.
(13) Zeng, W.; Wang, Y. H.; Han, S. C.; Chen, W. B.; Li, G.; Wang, Y. Z.; Wen, Y. Desigh, Synthesis and Characterization of a Novel Yellow Long-Persistent Phosphor: Ca_2BO_3Cl: Eu^{2+}, Dy^{3+}. *J. Mater. Chem. C* **2013**, *1*, 3004−3011.
(14) Ju, Z. H.; Wei, R. P.; Zheng, J. G.; Gao, X. P.; Zhang, S. H.; Liu, W. S. Synthesis and Phosphorescence Mechanism of a Reddish Orange Emissive Long Afterglow Phosphor Sm^{3+}-Doped Ca_2 SnO_4. *Appl. Phys. Lett.* **2011**, *98*, 121906.
(15) Qiu, Z. F.; Zhou, Y. Y.; Lü, M. K.; Zhang, A. Y.; Ma, Q. Combustion Synthesis of Long Persistent Luminescent MAl_2O_4: Eu^{2+}, R^{3+} (M=Sr, Ba, Ca, R= Dy, Nd and La) Nanoparticles and Luminescence Mechanism Research. *Acta Mater.* **2007**, *55*, 2615−2620.
(16) Ganesh, N.; Zhang, W.; Mathias, P. C.; Chow, E.; J. Soares, A.; Malyarchuk, V.; Smith, A. D.; Cunningham, B. T. Enhanced Fluorescence Emission From Quantum Dots on a Photonic Crystal Surface. *Nat. Nanotechnol.* **2007**, *2*, 515−520.
(17) Zhao, Y. J.; Xie, Z. Y.; Gu, H. C.; Zhu, C.; Gu, Z. Z. Bio-Inspired Variable Structural Color Materials. *Chem. Soc. Rev.* **2012**, *41*, 3297−3317.
(18) Puzzo, D. P.; Helander, M. G.; O'Brien, P. G.; Wang, Z. B.; Soheilnia, N.; Kherani, N.; Lu, Z. H.; Ozin, G. A. Organic Light-Emitting Diode Microcavities from Transparent Conducting Metal Oxide Photonic Crystal. *Nano Lett.* **2011**, *11*, 1457−1462.
(19) O'Brien, P. G.; Kherani, N. P.; Chutinan, A.; Ozin, G. A.; John, S.; Zukotynski, S. Silicon Photovoltaics Using Conductign Photonic Crystal Back-Reflectors. *Adv. Mater.* **2008**, *20*, 1577−1582.
(20) Li, Z. X.; Li, L. L.; Zhou, H. P.; Yuan, Q.; Chen, C.; Sun, L. D.; Yan, C. H. Color Modification Action of An Upconversion Photonic Crystal. *Chem. Commun.* **2009**, 6616−6618.
(21) Schäfer, C. G.; Gallei, M.; Zahn, J. T.; Engelhardt, J.; Hellmann, G. P.; Rehahn, M. Reversible Light-, Thermo-, and Mechano-Responsive Elastomeric Polymer Opal Films. *Chem. Mater.* **2013**, *25*, 2309−2318.
(22) Xu, H.; Wu, P.; Zhu, C.; Elbaz, A.; Gu, Z. Z. Photonic Crystal for Gas Sensing. *J. Mater. Chem. C* **2013**, *1*, 6087−6098.
(23) Xu, H.; Cao, K. D.; Ding, H. B.; Zhong, Q. F.; Gu, H. C.; Xie, Z. Y.; Zhao, Y. J.; Gu, Z. Z. Spherical Porphyrin Sensor Array Based On Encoded Colloical Crystal Beads for VOC Vapor Detection. *ACS Appl. Mater. Interfaces* **2012**, *4*, 6752−6757.
(24) He, L.; Wang, M. S.; Ge, J. P.; Yin, Y. D. Magnetic Assembly Route to Colloidal Responsive Photonic Nanostructures. *Acc. Chem. Res.* **2012**, *45*, 1431−1440.
(25) Hu, Y. X.; He, L.; Yin, Y. D. Charge Stabilization of Superparamagnetic Colloids for High-Performance Responsive Photonic Structures. *Small* **2012**, *8*, 3795−3799.
(26) Tao, C. A.; Zhu, W.; An, Q.; Li, G. T. Theoretical Demonstration of Efficiency Improvement of Dye-Sensitized Solar Cells with Double-Inverse Opal as Mirrors. *J. Phys. Chem. C* **2010**, *114*, 10641−10647.
(27) Tao, C. A.; Zhu, W.; An, Q.; Yang, H. W.; Li, W. N.; Lin, C. X.; Yang, F. Z.; Li, G. T. Coupling of Nanoparticle Plasmons with Colloidal Photonic Crystals as a New Strategy to Efficiently Enhance Fluorescence. *J. Phys. Chem. C* **2011**, *115*, 20053−20060.
(28) Scotognella, F.; Puzzo, D. P.; Monguzzi, A.; Wiersma, D. S.; Maschke, D.; Tubino, R.; Ozin, G. A. Nanoparticle One-Dimensional Photonic Crystal Dye Laser. *Small* **2009**, *5*, 2048−2052.
(29) Huang, C. S.; George, S.; Lu, M.; Chaudhery, V.; Tan, R.; Zangar, R. C.; Cunningham, B. T. Application of Photonic Crystal Enhanced Fluorescence to Cancer Biomarker Microarrays. *Anal. Chem.* **2011**, *83*, 1425−1430.
(30) Shen, W. Z.; Li, M. Z.; Xu, L.; Wang, S. T.; Jiang, L.; Song, Y. L.; Zhu, D. B. Highly Effective Protein Detection for Avidin-Biotin System Based on Colloical Photonic Crystals Enhanced Fluoroimmunoassay. *Biosens. Bioelectron.* **2011**, *26*, 2165−2170.
(31) Li, M. Z.; He, F.; Liao, Q.; Liu, J.; Xu, L.; Jiang, L.; Song, Y. L.; Wang, S.; Zhu, D. B. Ultrasensitive DNA Detection Using Photonic Crystal. *Angew. Chem. Int. Ed.* **2008**, *47*, 7258−7262.
(32) Shi, X. D.; Li, M. Z.; Ye, C. Q.; Shen, W. Z.; Wen, Y. Q.; Chen, L. F.; Yang, Q.; Shi, L.; Jiang, L.; Song, Y. L. Photonic Crystal Boosted Chemiluminescence Reaction. *Laser Photonics Rev.* **2013**, *7*, L39−L43.
(33) Wang, J. X.; Wen, Y. Q.; Ge, H. L.; Sun, Z. W.; Zheng, Y. M.; Song, Y. L.; Jiang, L. Control Over the Wettability of Colloidal Crystal Films by Assembly Temperature. *Macromol. Chem. Phys.* **2006**, *207*, 596−604.
(34) Jiang, P.; Bertone, J. F.; Hwang, K. S.; Colvin, V. L. Single Crystal Colloidal Multilayers of Controlled Thickness. *Chem. Mater.* **1999**, *11*, 2132−2140.
(35) Hwang, K. S.; Kang, B. A.; Kim, S. D.; Hwangbo, S.; Kim, J. T. Cost Effective Electrostatic-Sprayed $SrAl_2O_4$: Eu^{2+} Phosphor Coatings by Using Salted Sol-Gel Derived Solution. *Bull. Mater. Sci.* **2011**, *34*, 1059−1062.
(36) Huang, Y.; Zhou, J. M.; Su, B.; Shi, L.; Wang, J. X.; Chen, S. R.; Wang, L. B.; Zi, J.; Song, Y. L.; Jiang, L. Colloidal Photonic Crystal with Narrow Stopbands Assembled from Low-Adhesive Superhydrophobic Substrates. *J. Am. Chem. Soc.* **2012**, *134*, 17053−17058.
(37) Shi, S. Y.; Chen, C. H.; Prather, D. W. Plane-Wave Expansion Method for Calculating Band Structure of Photonic Crystal Slabs with Perfectly Matched Layers. *J. Opt. Soc. Am. A* **2004**, *21*, 1769−1775.